Supporting Information

Perylene Diimide Functionalized Nano Silica: Green Emissive Material for Selective Probing and Remediation of 4-Nitrocatechol, Ru^{3+}, and Cu^{2+} with Biosensing Applications†

Sanjay Yadav,*[ac] Nishu Choudhary,[ac] Avinash T. Vasave,[ac] Vasavdutta Sonpal,[bc] and Alok Ranjan Paital*[ac]

[a]*Salt and Marine Chemicals Division, CSIR-Central Salt & Marine Chemicals Research Institute, G.B. Marg, Bhavnagar-364002, Gujarat, India.*

E-mail: arpaital@csmcri.res.in;sychem00700@gmail.com

[b]*Analytical and Environmental Science Division & Centralized Instrument Facility, CSIR-Central Salt & Marine Chemicals Research Institute, Bhavnagar 364 002, Gujarat, India.*

[c]*Academy of Scientific and Innovative Research (AcSIR), Ghaziabad-201002, India.*

Materials: For chemical processing all the chemicals and reagents were used as supplied without further purification. The synthetic procedures were done using dry solvents. Perylene dianhydride tetracarboxylic anhydride (PTCDA), Hydrazine monohydrate, AOT (dioctyl sodium sulfosuccinate), Trimethylbenzene, Maleic anhydride, TEOS, 2-aminobenzimidazole, Choranil, 3-Chloropropyltriethoxysilane (3-CPTES), NaOH, HCl, HEPES Buffer, Isopropanol and screened nitro analytes were purchased from Merck (Sigma) And TCI Chemicals Private Ltd. Dry solvents, reagents, chloride salts of cations and potassium or sodium salts of anions were purchased from Spectrochem Private Ltd.

Instrumentation: To obtain the optical parameters, the UV-Vis absorption and fluorescence emission spectra were obtained using the Shimadzu UV 3101PC spectrophotometer and Edinburg Instruments model Xe-900 with a 380 nm excitation source in an aqueous dispersion medium. Structural characterization involved FTIR spectra measured using a Perkin-Elmer GX spectrophotometer with KBr pellets. Surface area measurements were conducted with the Micromeritics 3 FLEX instrument, activating the sample at 65 °C for 50 minutes before analysis. The FeSEM (SEM-Leo series 1420 VP) with INCA was used for surface morphology and transmission electron microscopy (TEM) on a JEOL JEM 2100 microscope with Lacey carbon-coated grids. X-ray photoelectron spectroscopy (XPS) for chemical and surface state analysis was performed with a Thermo Fisher Nexsa spectrophotometer, using monochromated Al Kα radiation at 1486.6 eV. The specific metal ion concentrations were determined using the ICP-MS Thermo Fisher iCAP Qnova series instrument, with samples filtered through Thermo Fisher syringe filters (0.45 μm). Powder X-ray diffraction profiles were recorded on a Rigaku MiniFlex-II powder diffractometer with a scan rate of 1° per minute. Fluorescence lifetime measurements were carried out using TSPC experiments on an Edinburg Instruments OB 920

fluorescence spectrophotometer, equipped with a pulse diode laser (Laser-EPLED-380 nm) as the excitation source.

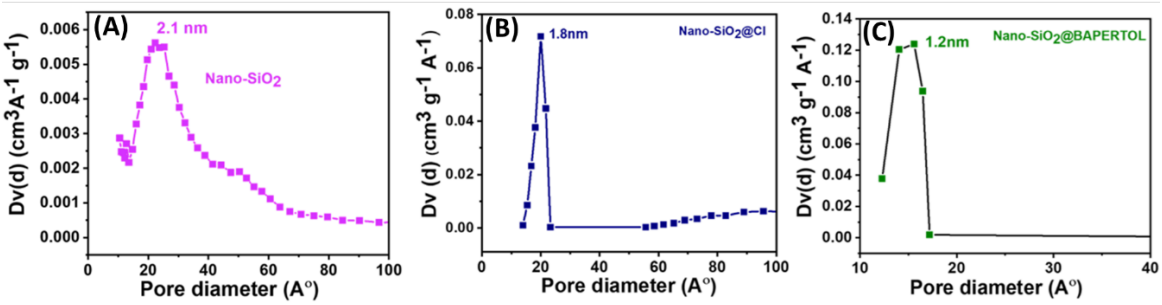

Figure S1. (A-C) The pore size parameters of the synthesized materials Nano-SiO_2, Nano-SiO_2@Cl, and the final material Nano-SiO_2@BAPERTOL.

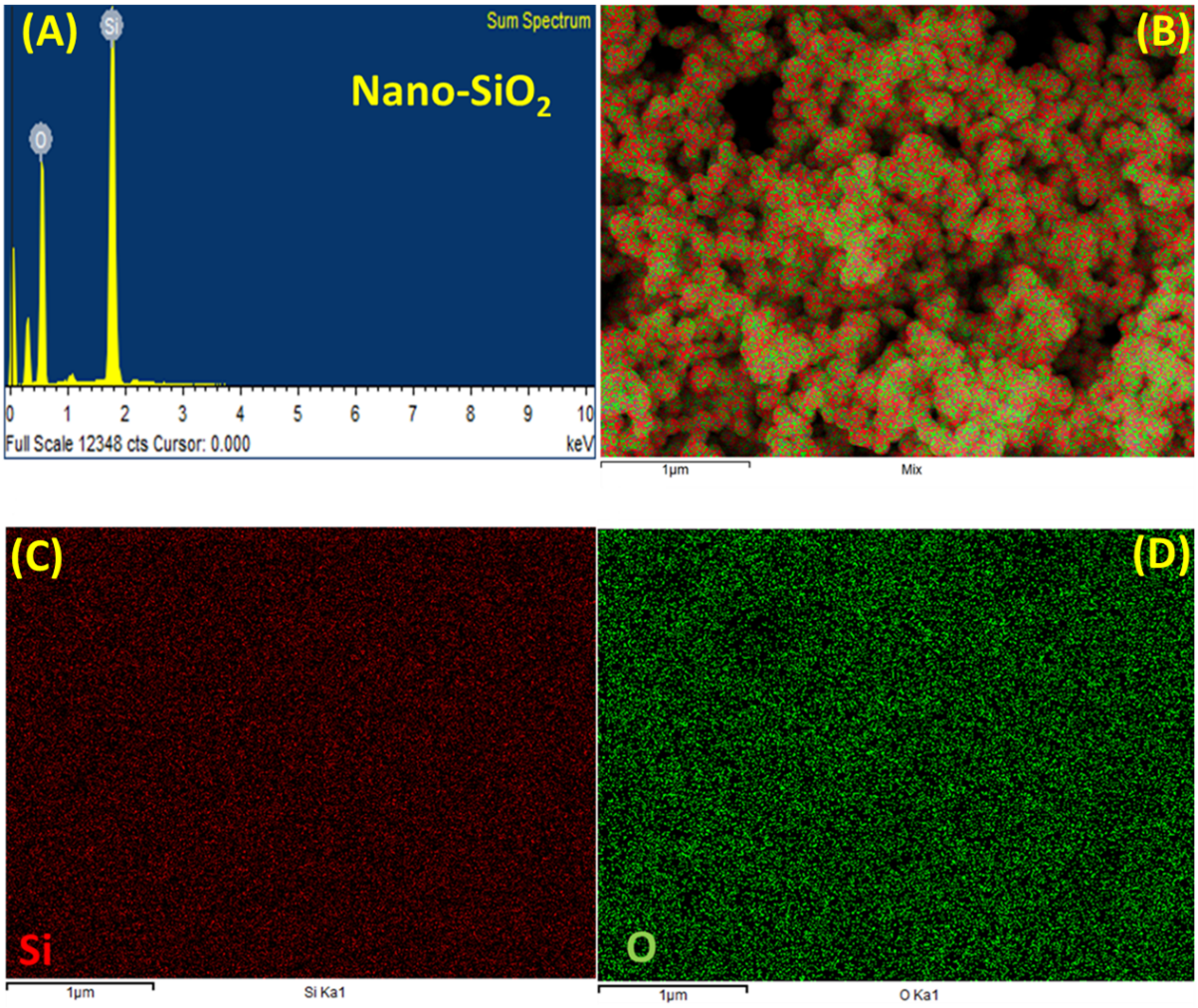

Fig. S2 (A) The EDX analysis of the synthesized nano silica (Nano-SiO_2); (B-D) The elemental color mapping of the synthesized nano silica (Nano-SiO_2).

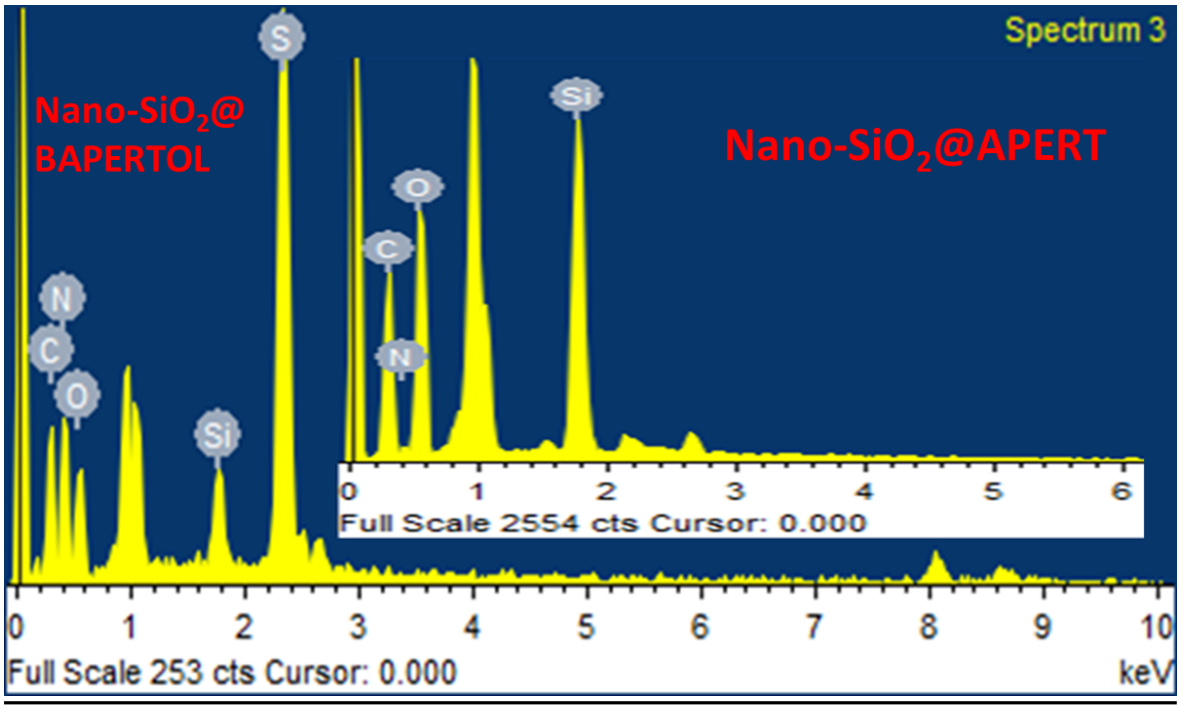

Fig. S3. The comparison of the EDX analysis of the intermediate Nano-SiO_2@APERT (inset)and the final material Nano-SiO_2@BAPERTOL.

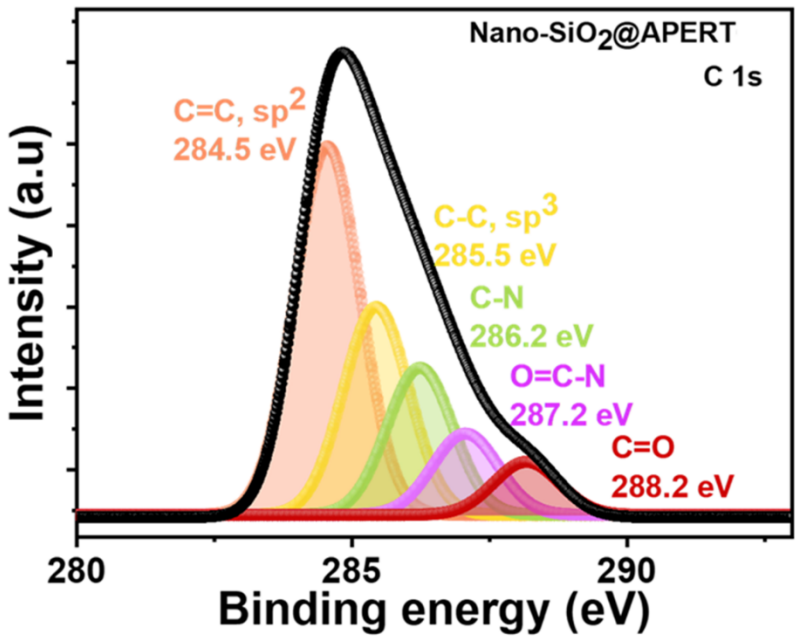

Fig. S4 The XPS core shell C 1s spectra of the intermediate material Nano-SiO_2@APERT.

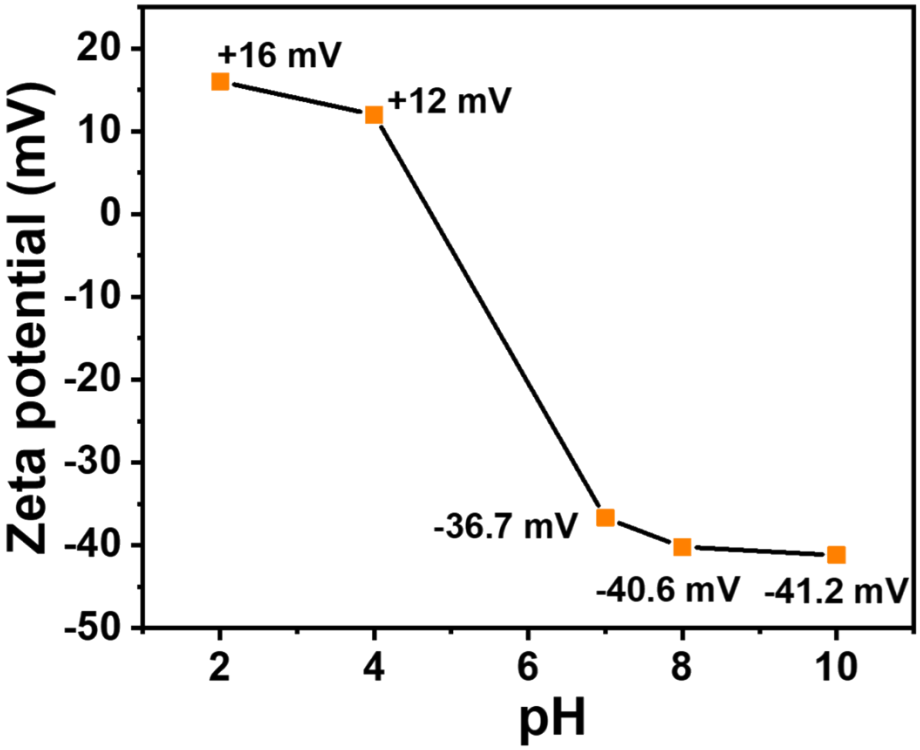

Fig. S5 The Zeta potential profile of the final material Nano-SiO_2@BAPERTOL.

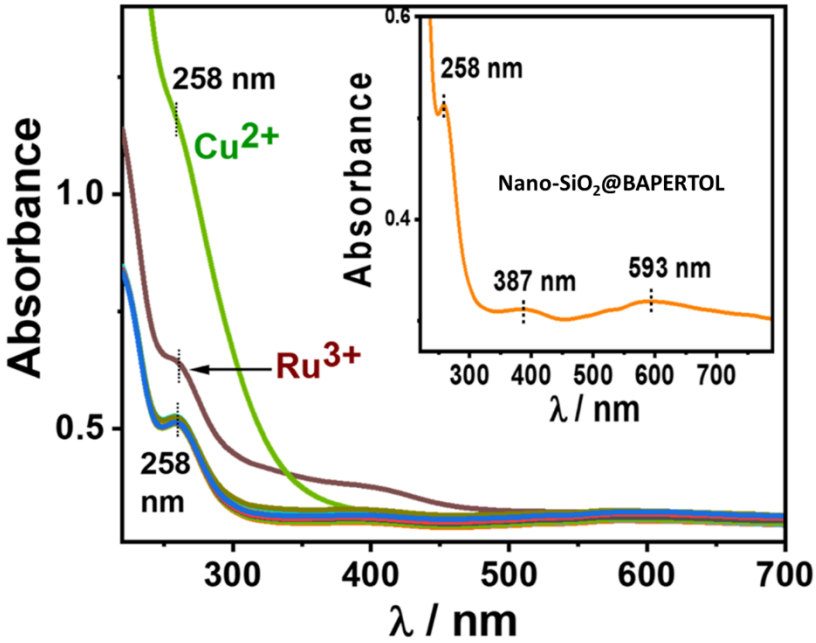

Fig. S6 The UV-Vis selectivity profile of the final material Nano-SiO_2@BAPERTOL.

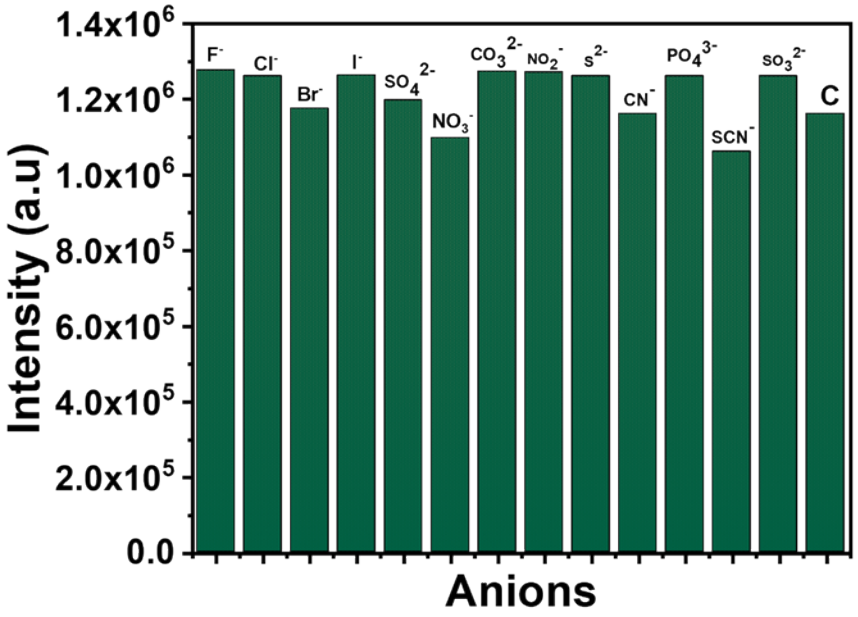

Fig. S7 The Fluorescence emission intensity of the final material in the presence of anions.

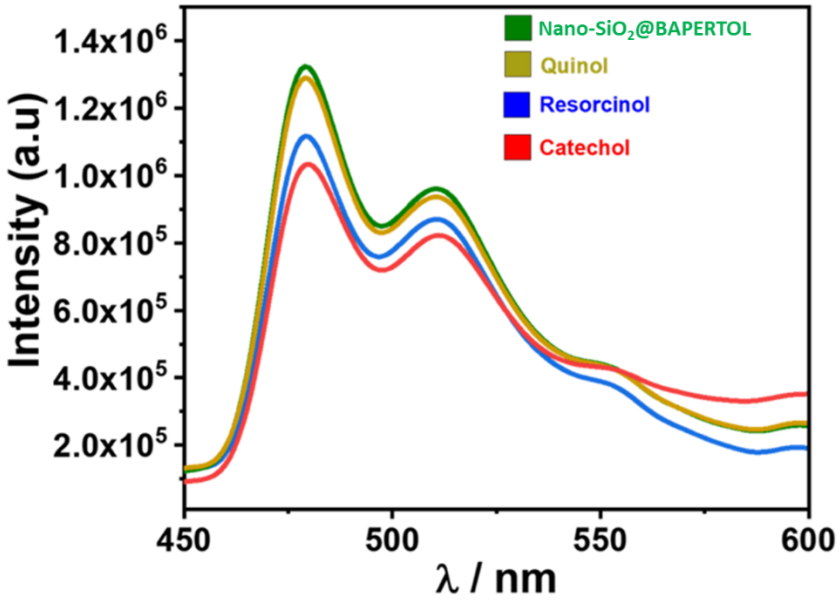

Fig. S8 The Fluorescence selectivity profile of the material in the presence of diols.

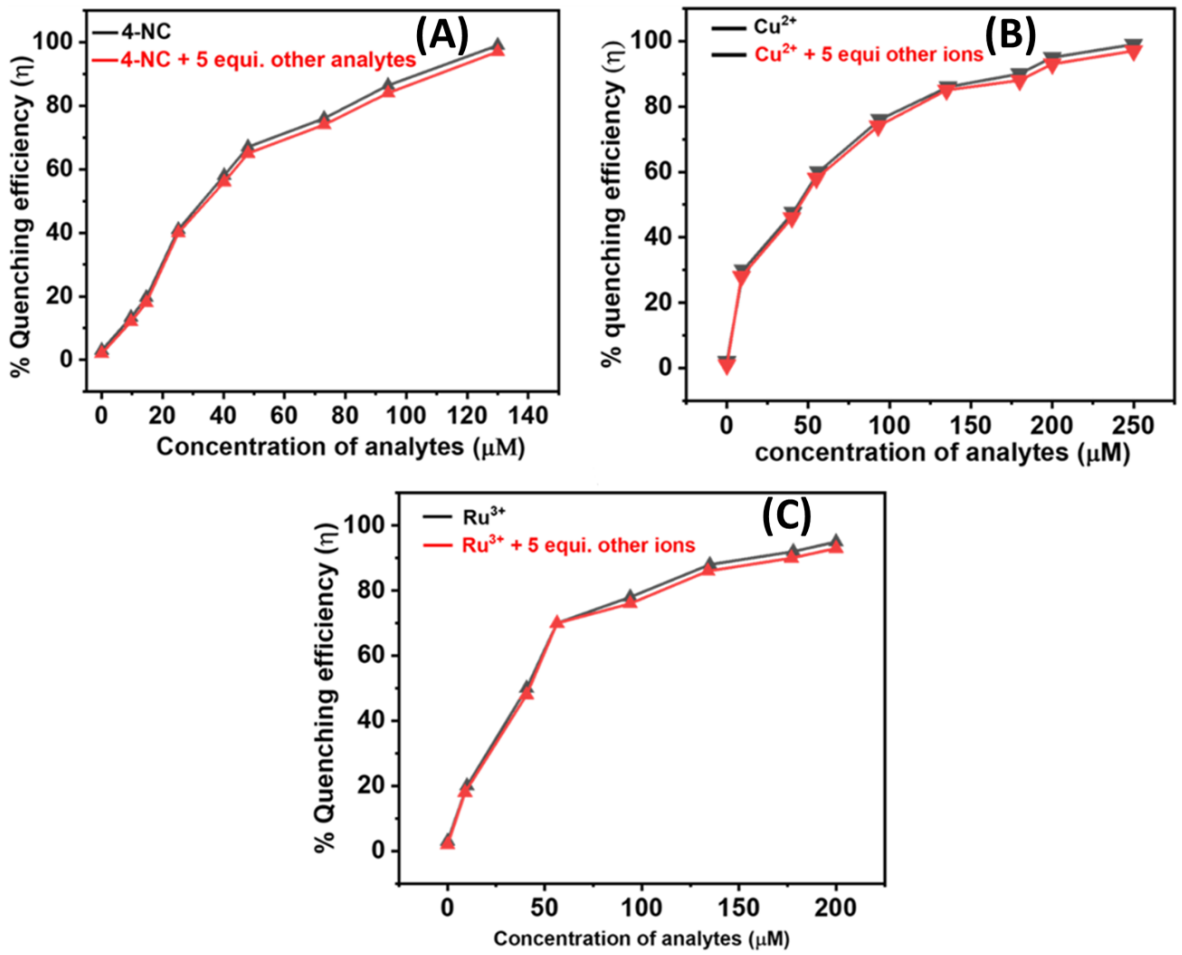

Fig. S9 (A-C) The interference study of the material in the presence of other analytes and ions (except the interfering ions).

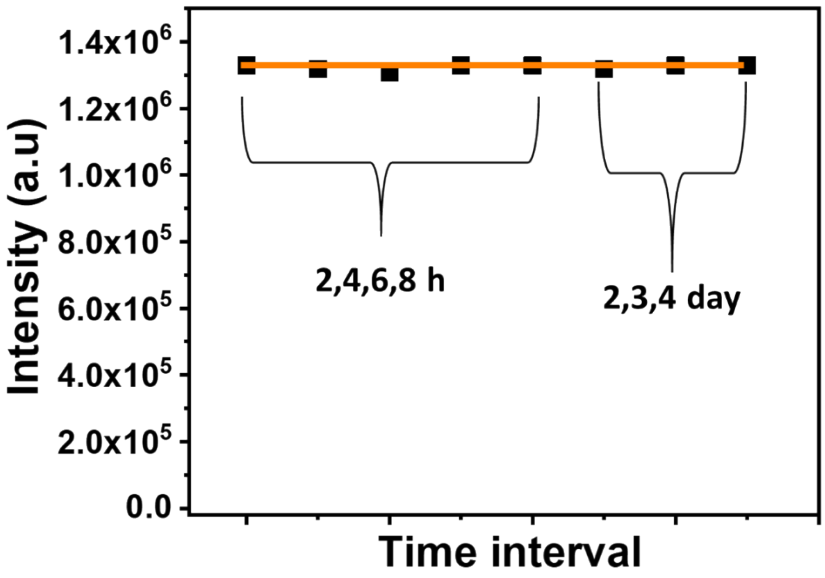

Fig. S10 The fluorescence emission stability of the final material Nano-SiO_2@BAPERTOL.

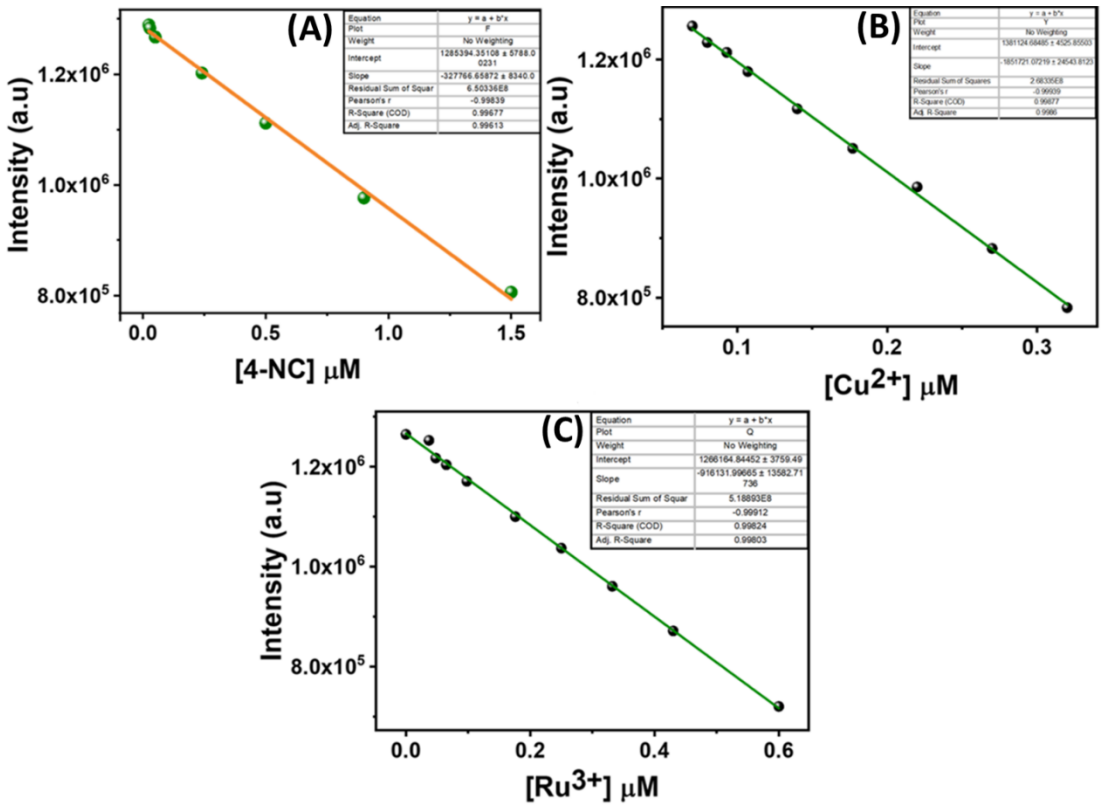

Fig. S11 (A-C) The limit of detection plots (LOD) of the materials towards specific analytes (4-NC, Cu^{2+} & Ru^{3+}).

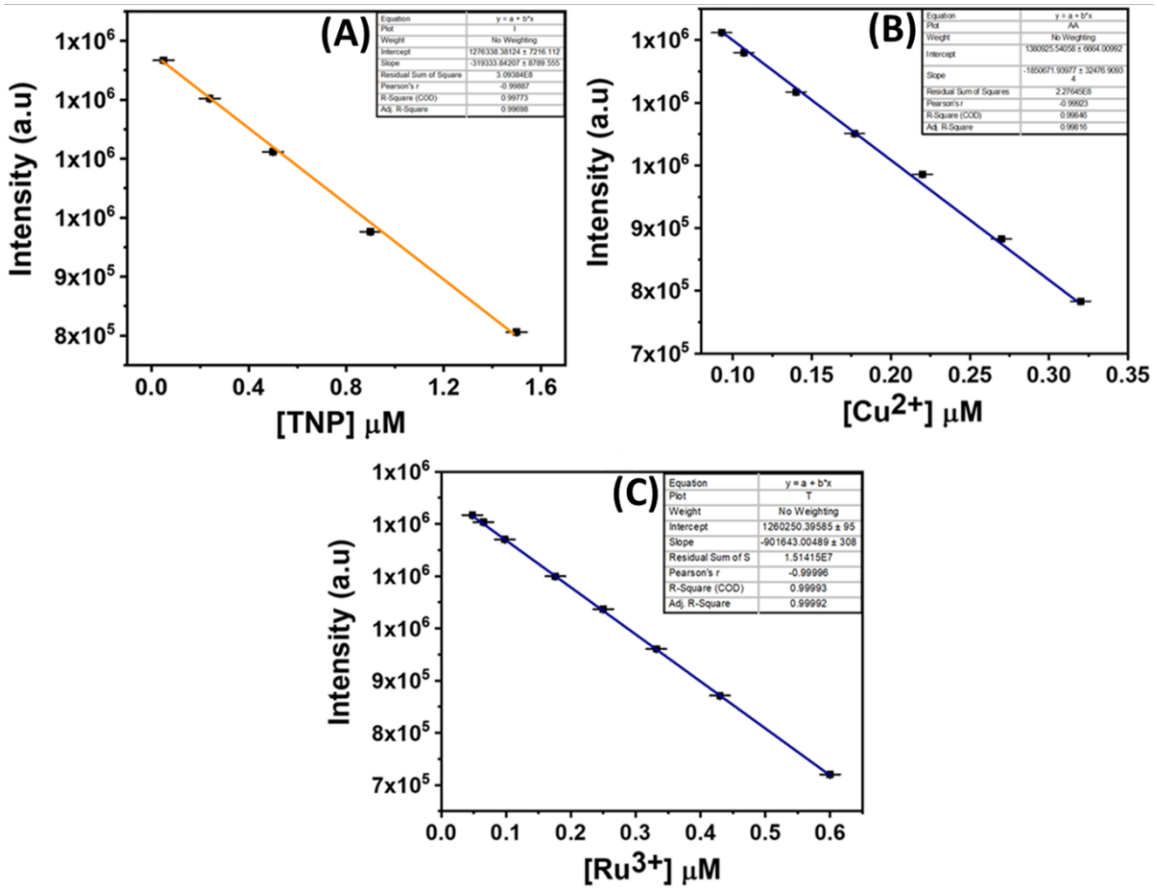

Fig. S12 (A-C) The Linear range plot (L-R) of the materials towards specific analytes (4-NC, Cu^{2+} & Ru^{3+}).

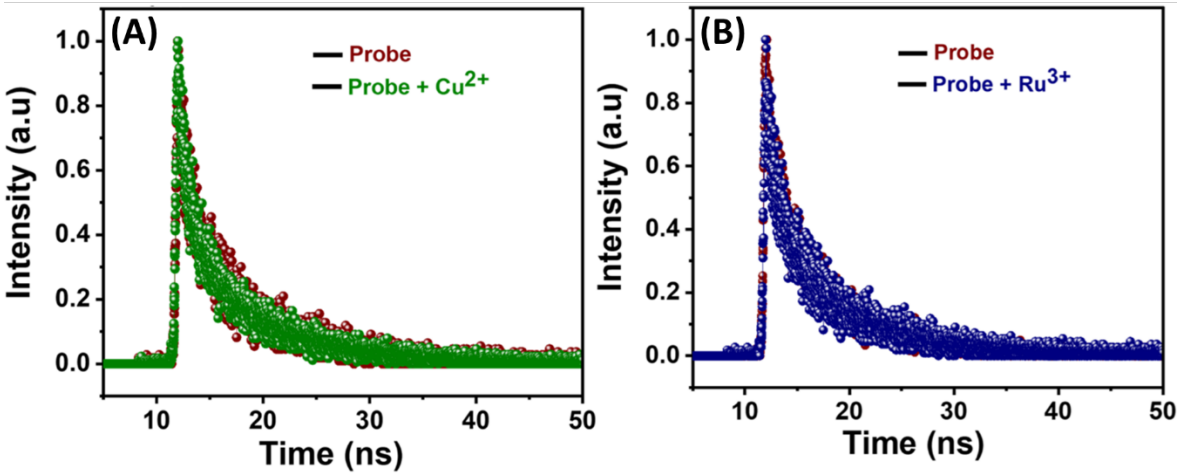

Fig. S13 (A-B) The Time correlated single photon counting (TCSPC) plots of the material towards Cu^{2+} and Ru^{3+} ions.

Table S1. The fluorescence lifetime measurements of the material with the specific analytes

Sample	τ (ns)	Percentage	χ^2
Nano-SiO_2@BAPERTOL (Probe)	3.89	100	0.98
Probe + Cu^{2+}	3.84	100	1.02
Probe + Ru^{3+}	3.86	100	0.99
Probe + 4-NC 5 (μM)	3.65	100	1.10
Probe + 4-NC (10 μM)	3.12	100	0.99
Probe + 4-NC (15 μM)	2.87	100	0.99
Probe + 4-NC (20 μM)	2.42	100	0.98

Table S2. The Competitive extraction performance table.

Metal ions	C_i = (Initial concentration)	C_f = (Final concentration)	% R = Ci – C_f / Ci ×100
Li^+	25.01	24.62	Nil
Na^+	24.58	23.38	Nil
Cs^+	25.16	25.43	Nil
Mg^{2+}	24.64	23.87	Nil
Ca^{2+}	22.84	22.93	Nil
Sr^{2+}	23.66	22.39	Nil
Cr^{3+}	24.25	24.51	Nil
Mn^{2+}	24.83	23.93	Nil
Fe^{3+}	23.56	22.72	Nil
Co^{2+}	25.13	23.47	Nil
Ni^{2+}	23.80	22.22	Nil
Cu^{2+}	25.23	0.98	96.11 %
Zn^{2+}	24.98	23.90	Nil
Pd^{2+}	24.85	22.71	Nil
Ru^{3+}	23.92	2.45	89.75 %
Cd^{2+}	23.33	22.33	Nil
Hg^{2+}	24.81	23.55	Nil
As^{3+}	25.12	23.72	Nil

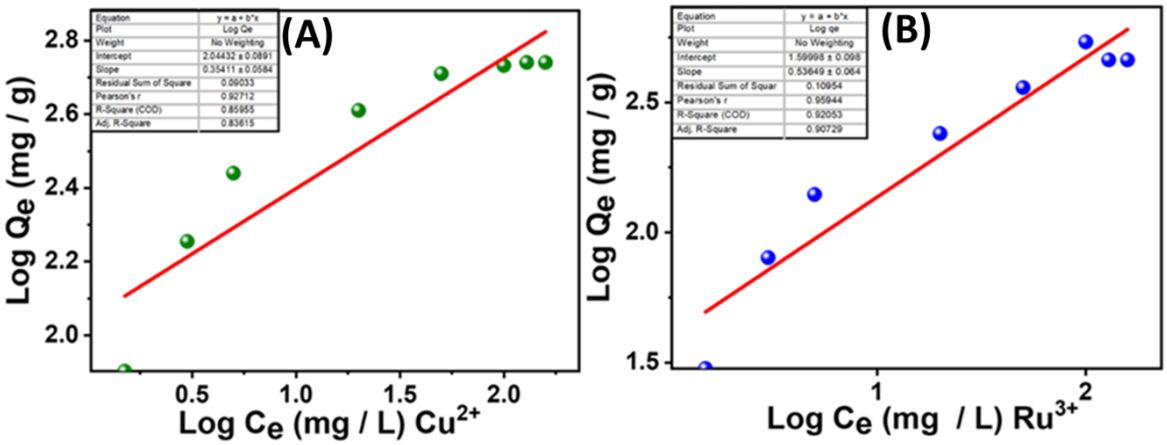

Fig. S14 (A-B) The Freundlich adsorption isotherm plot of the material towards specific ions.

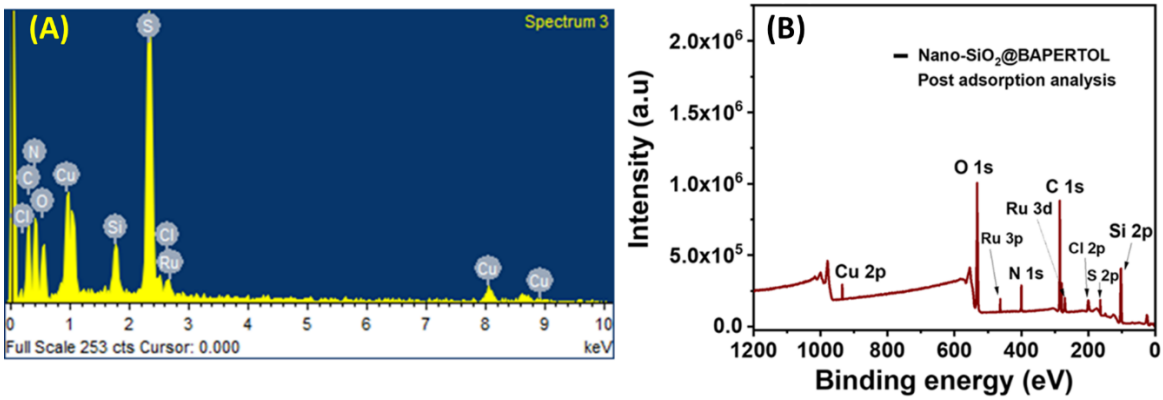

Fig. S15 (A, B) The EDX and XPS analysis of the material post adsorption of the specific analytes.

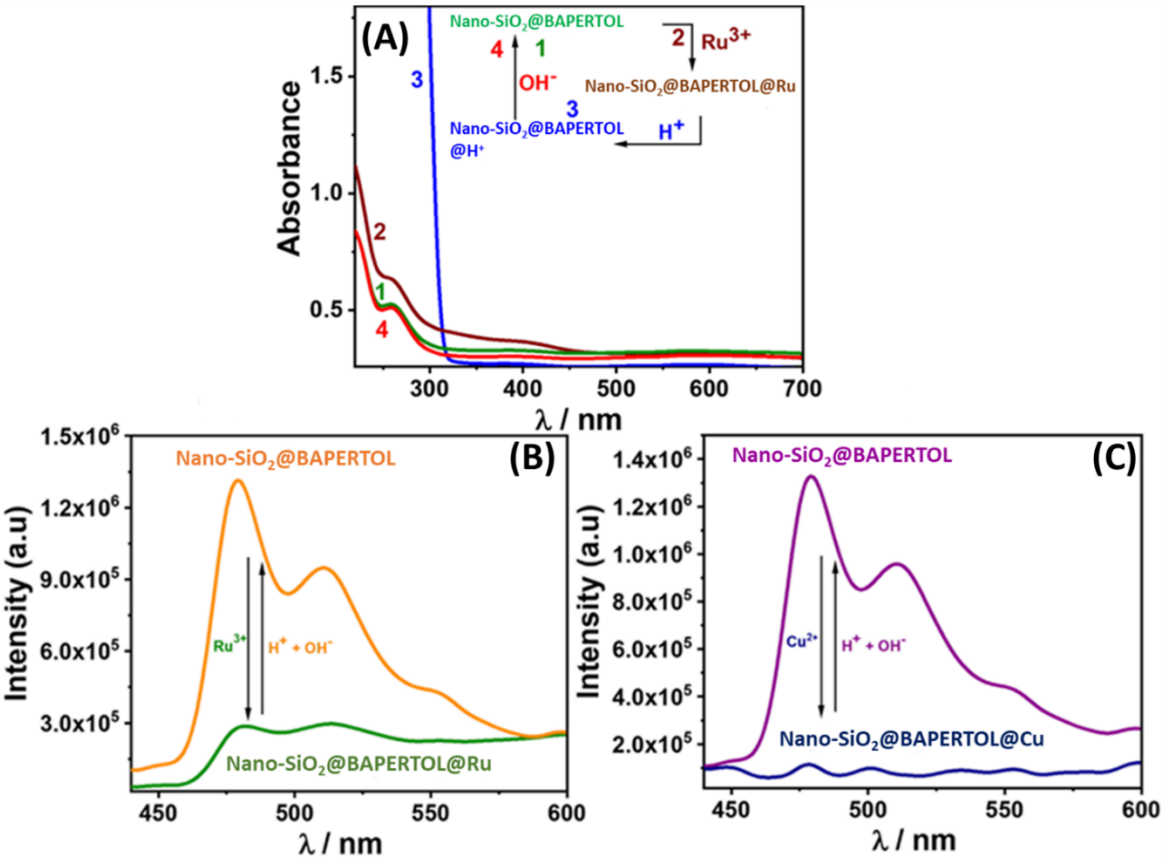

Fig. S16 (A, B) The UV-Vis reversibility study and fluorescence tracking of the material toward Ru^{3+} ions; (C) The fluorescence tracking during regeneration of the material towards Cu^{2+} ions.

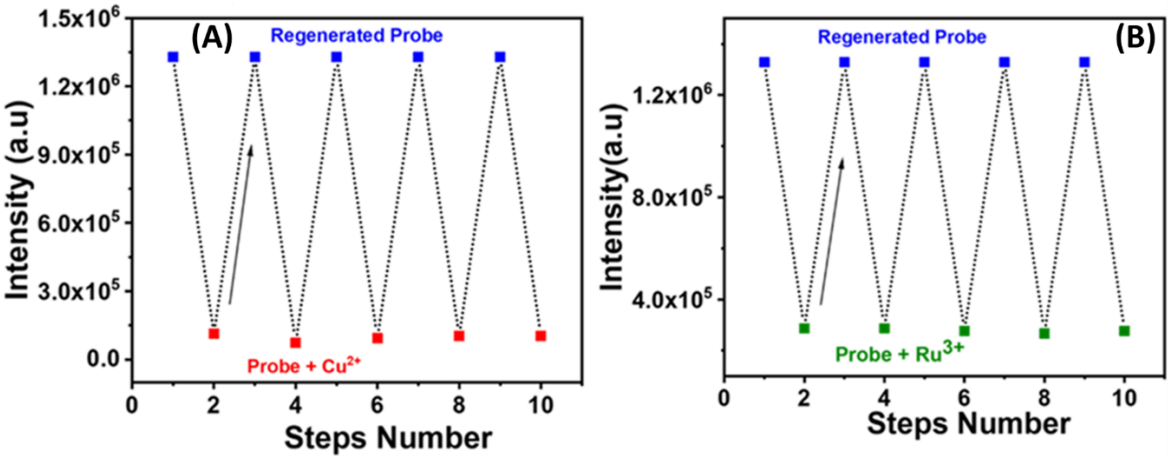

Fig. S17 (A-B) The Fluorescence emission intensity tracking during regeneration of the material towards the specific ions.

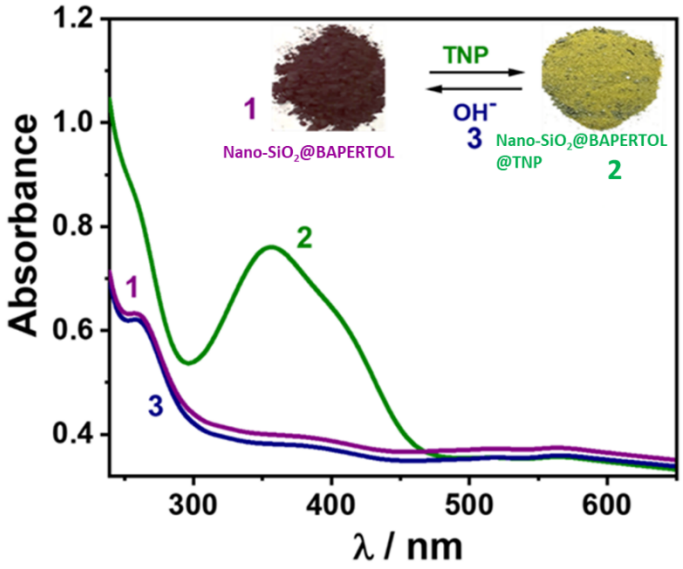

Fig. S18 The UV-Vis regeneration of the material towards TNP, inset: color change picture during regeneration.

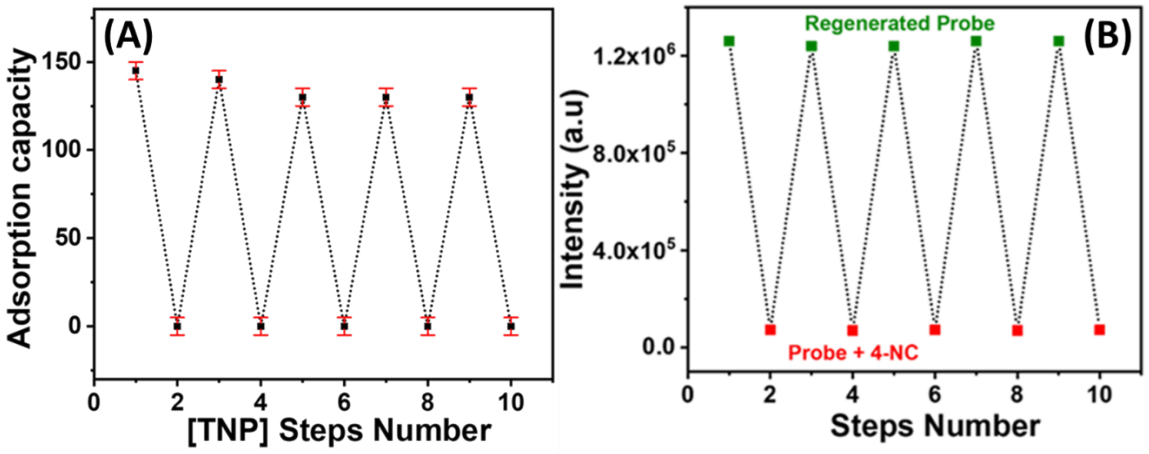

Fig. S19 (A) The adsorption capacity of the material during regeneration towards TNP; (B) The fluorescence tracking during regeneration of the material towards 4-NC.

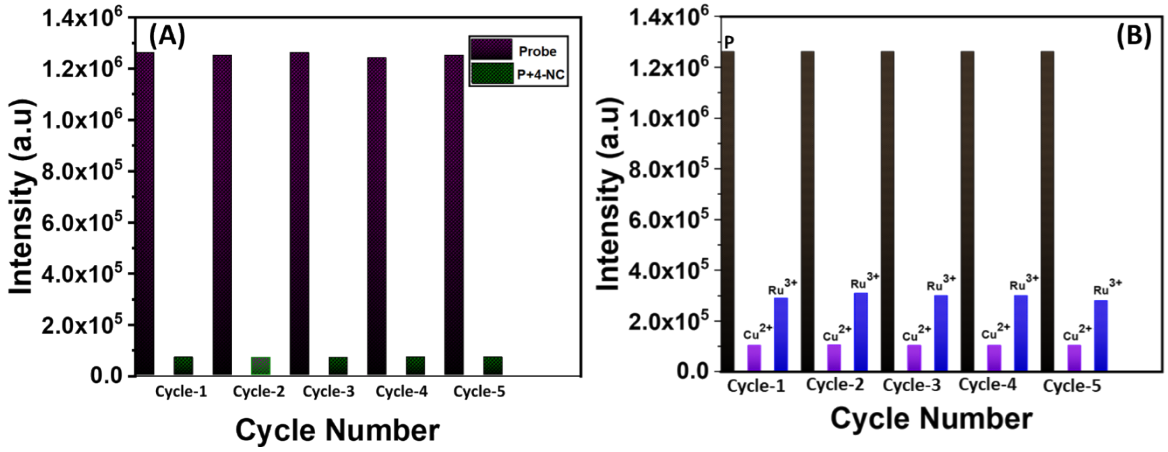

Fig. S20 The fluorescence quenching efficiency plots of the regenerated material during regeneration experiments over 5 detection cycles.

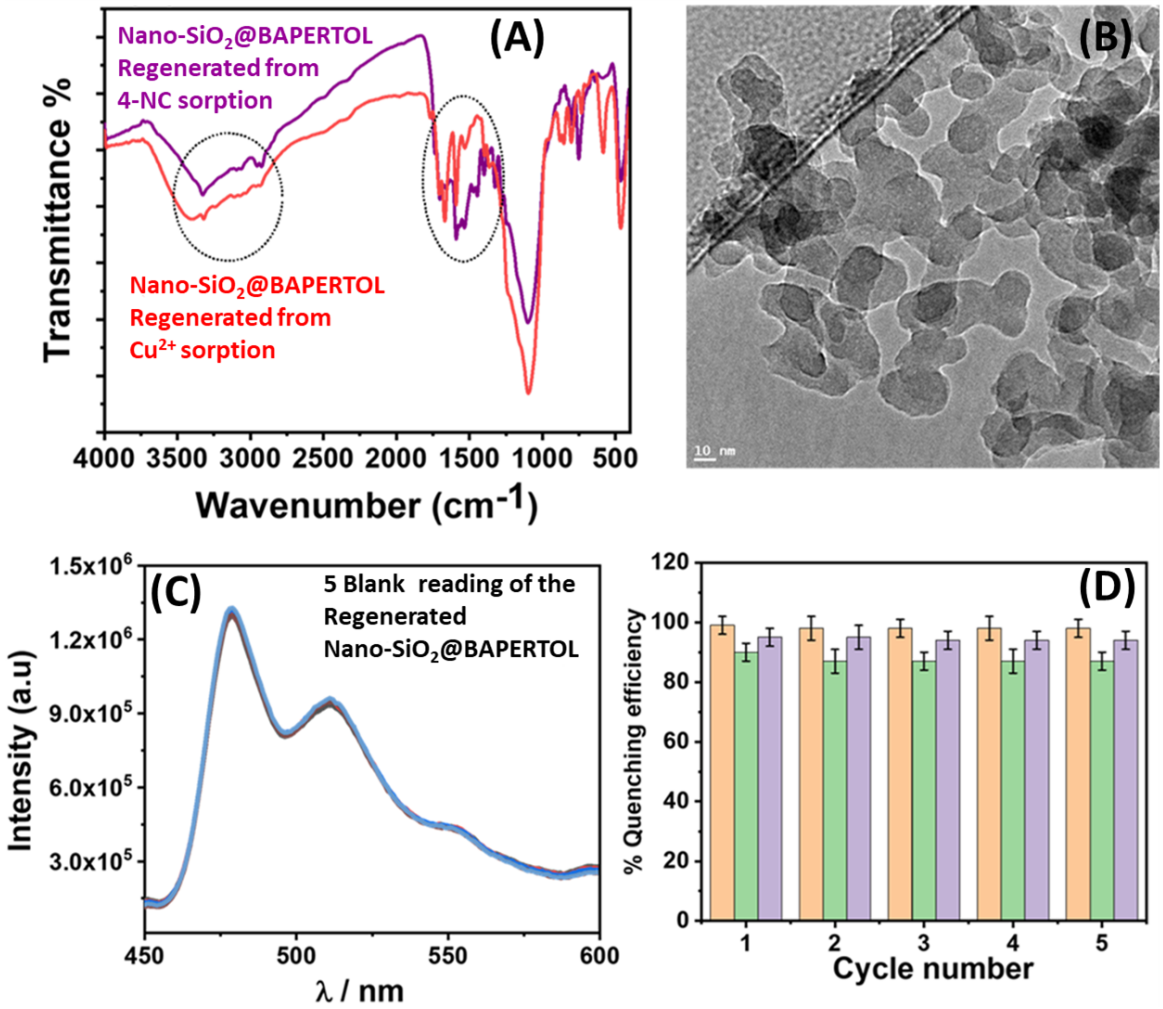

Fig. S21 (A) The FTIR comparison of the original and regenerated material showing intact functionality; (B) The HR-TEM of the regenerated material exhibits intact morphology; (C, D) The fluorescence activity and quenching behavior of the regenerated material towards specific analytes show optical behavior similar to that of control experiments.

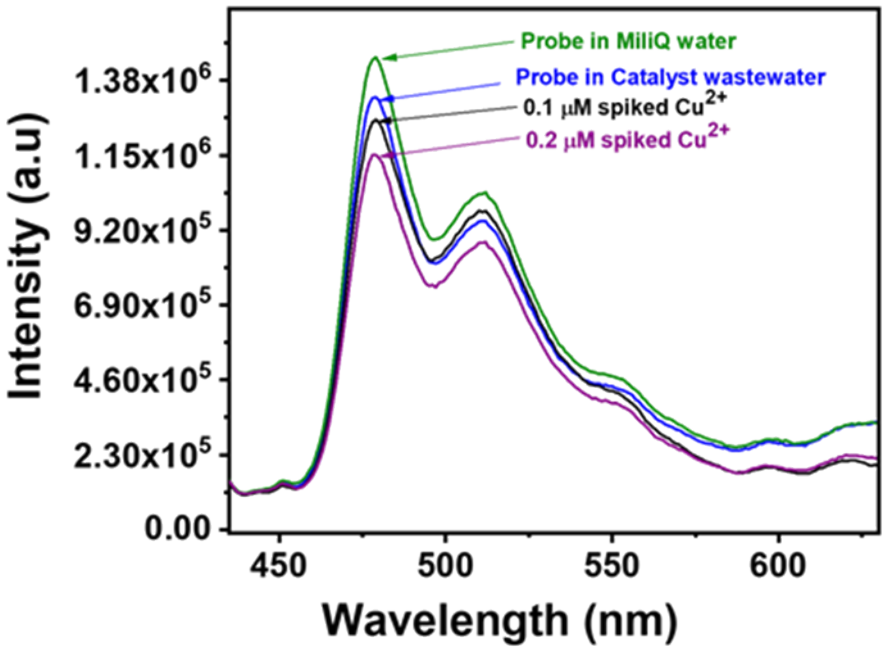

Fig. S22 The Fluorescence emission intensity of the material with catalyst wastewater and spike Cu^{2+} ions.

Table S3 The real sample quantification of Cu^{2+} ions

Analyte	Proposed (μM)	Spiked (μM)	Found (μM)	Recovery %	RSD (N=2)
Cu^{2+}	0.09	0.1	0.193	101.57	0.54
		0.2	0.30	103.44	1.23

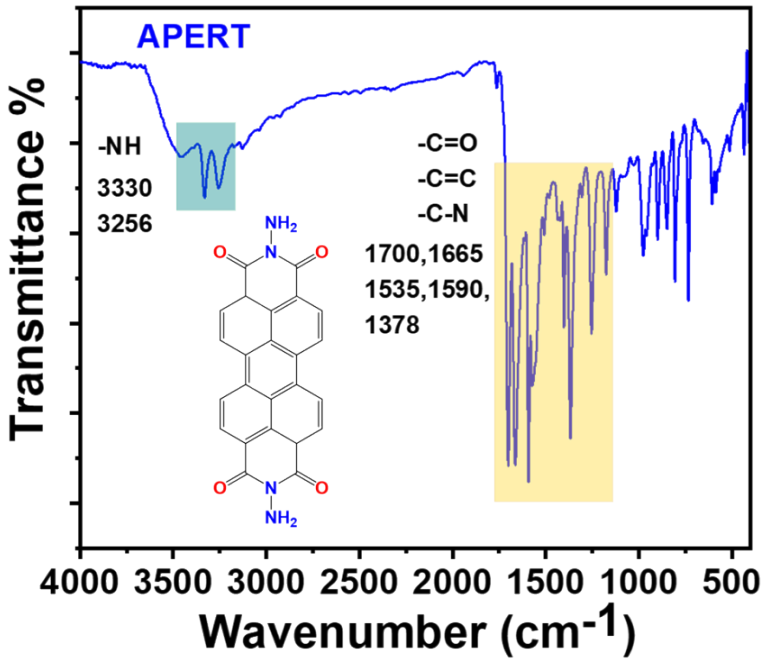

Fig. S23 The FTIR spectrum of the synthesized APERT ligand.

Table S4. The comparison of detection parameters of the material with the reported literature

Material	Specific Analyte	Fluorescence Response	LOD	Ref
Caprolactone-Based Biodegradable Polymer	Cu^{2+}	Ratiometric response	29 nM and 0.3 μM	S1
Mesoporous SBA-15 nanosensor	Cu^{2+}	Turn OFF	0.19 μM	S2
Functionalized Mesoporous Silica	Cu^{2+}	Turn OFF	6 ppb	S3
NIR Luminescent Ru–LPMSN Hybrid Materials	Cu^{2+}	Turn OFF	10.0×10^{-9} M	S4

Silsesquioxane-based fluorescent nanoporous polymer	Ru^{3+}	Turn OFF	5.2×10^{-6} mol L^{-1}	S5
Zinc (II)-based coordination polymer encapsulated Tb^{3+}	Ru^{3+}	Turn OFF	0.27 μM	S6
A Highly Stable 3D Luminescent Indium–Polycarboxylic Framework	Ru^{3+}	Turn OFF	0.26 ppm	S7
A novel stable 3D luminescent uranyl complex	Ru^{3+}	Turn OFF	21.53 μM	S8
Functionalized DFNS	4-NC, Cu^{2+}	Turn OFF	0.090 μM, 0.44 μM	47
Perylene Functionalized Nano-silica	**4-NC, Cu^{2+} & Ru^{3+}**	**Turn OFF**	**4.34, 0.43, 0.56 nM**	**This work**

Supporting References

S1 N. Das, T. Samanta, S. Gautam, K. Khan, S. Roy and R. Shunmugam, *ACS Polym. Au*, 2024, 4, 247–254.

S2 Y. Zhang, T. Zhu, H. Wang, L. Zheng, M. Chen and W. Wang, *Dalt. Trans.*, 2022, 51, 7210–7222.

S3 S. Chatterjee, H. Gohil, I. Raval, S. Chatterjee and A. R. Paital, *Small*, 2019, 15, 1804749

S4 F. Chen, F. Xiao, W. Zhang, C. Lin and Y. Wu, *ACS Appl. Mater. Interfaces*, 2018, 10, 26964–26971.

S5 Y. Yan, H. Yang and H. Liu, *Sensors Actuators B Chem.*, 2020, 319, 128154.

S6 Y. Wu, D. Liu, M. Lin and J. Qian, *RSC Adv.*, 2020, 10, 6022–6029.

S7 N. Du, J. Song, S. Li, Y.-X. Chi, F.-Y. Bai and Y.-H. Xing, *ACS Appl. Mater. Interfaces*, 2016, 8, 28718–28726.

S8 H.-H. Tian, L.-T. Chen, R.-L. Zhang, J.-S. Zhao, C.-Y. Liu and N. S. Weng, *J. Solid State Chem.*, 2018, 258, 674–681.